Mechanistic Origins of Methyl-Driven Overhauser DNP

Frédéric A. Perras,[a]* Yoh Matsuki,[b,c] Scott A. Southern,[a] Thierry Dubroca,[d] Dragos F. Flesariu,[e] Johan Van Tol,[d] Christos P. Constantinides,[f] Panayiotis A. Koutentis[e]

[a] Chemical and Biological Sciences Division, Ames National Laboratory, Ames, IA 50011, United States

[b] Institute for Protein Research, Osaka University, Suita, Osaka 565-0871, Japan

[c] Center for Quantum Information and Quantum Biology, Osaka University, Toyonaka, Osaka 560-0043, Japan

[d] National High Magnetic Field Laboratory, Florida State University, Tallahassee, FL 32310, United States

[e] Department of Chemistry, University of Cyprus, P.O. Box 20537, 1678 Nicosia, Cyprus

[f] Department of Natural Sciences, University of Michigan-Dearborn, Dearborn, Michigan 48128, United States

*fperras@ameslab.gov

Abstract

The Overhauser effect in the dynamic nuclear polarization (DNP) of non-conducting solids has drawn much attention due to the potential for efficient high-field DNP as well as a general interest in the underlying principles that enable the Overhauser effect in small molecules. We recently reported the observation of ^{1}H and ^{2}H Overhauser effects in H_3C- or D_3C-functionalized Blatter radical analogues which we presumed to be caused by methyl rotation. In this work, we look at the mechanism for methyl-driven Overhauser DNP in greater detail, considering methyl librations and tunneling, in addition to classical rotation. We predict the temperature dependence of these mechanisms using density functional theory and spin dynamics simulations. Comparisons with results from ultralow-temperature magic angle spinning (MAS)-DNP experiments revealed that cross-relaxation at temperatures above 60 K originates from both libration and rotation, while librations dominate at lower temperatures. Due to the zero-point vibrational nature of these motions, they are not quenched by very low temperatures, and methyl-driven Overhauser DNP is expected to increase in efficiency down to 0 K, predominantly due to increases in nuclear relaxation times.

I. Introduction

Dynamic nuclear polarization (DNP) is the prime hyperpolarization technique used in solid-state nuclear magnetic resonance (NMR) for sensitivity enhancement. In particular, it has become a pillar in structural investigations of interfaces and biomolecules.[1-9] There are three primary DNP mechanisms used in modern continuous-wave (CW) magic angle spinning (MAS)-DNP, namely, the solid effect (SE),[10,11] the cross-effect (CE),[12] and the Overhauser effect (OE).[13,14] Of these mechanisms, the CE is by far the most successful due to its use of fundamentally-allowed electron paramagnetic resonance (EPR) transitions and the ease with which polarizing agents can be designed to satisfy the 2-electron, 1-nuclear CE condition.[15-21] The OE also deals exclusively with fundamentally allowed EPR transitions but is less common in solids due to its stricter matching conditions. Specifically, the OE is triggered by electron-nuclear cross-relaxation which requires that the hyperfine interaction be modulated dynamically at the EPR frequency. Early work by Griffin and co-workers, however, highlighted the tremendous promise of OE DNP for high-field DNP due to the potential for using narrow-line radicals and frequency matching the dynamics to lead to higher performance at higher magnetic fields.[22]

1,3-Bisdiphenylene-2-phenylallyl (BDPA), the polarizing agent with which the OE in insulating solids was first observed,[22] can promote electron-nuclear cross-relaxation due to its properties as a mixed-valence compound. As explained by Pylaeva and co-workers, the electron-spin localization is coupled to the ground state vibrational wavefunction which features a double-welled potential, ultimately leading to the shuttling of the electron spin to either side of the molecule. This process modulates the hyperfine coupling for some ^{1}H spins at the vibrational frequency, which is in the range of typical EPR Larmor frequencies, thus enabling OE DNP.[23,24] This mechanism was later confirmed by the observation of strong Overhauser effects in other mixed valence radicals[25] in addition to deuteration experiments.[26,27]

We recently reported the observation of OE DNP with a radical that is not a mixed valence compound.[28] More specifically, we looked at 7-methyl-1,3-diphenyl-1,4-dihydrobenzo[*e*][1,2,4]triazin-4-yl (**1**), a Blatter-type radical[29] that was functionalized with a methyl group at C7 (Figure 1).[30-33] The absence of the methyl group, *i.e.*, the parent Blatter radical **2**, or its deuteration as in the 7-D_3C analogue **3**, leads to the elimination of the ^{1}H OEs in the former, and the appearance of ^{2}H OEs in the latter. We thus concluded that the enhancements likely originated from methyl rotation, which we found, using density functional theory (DFT) calculations, would fall in the expected range to support OE DNP.[28] Interestingly, reexamination of data acquired by Maly *et al.* over a decade ago suggests that this effect may have been originally discovered on the flavin mononucleotide semiquinone of flavodoxin.[34]

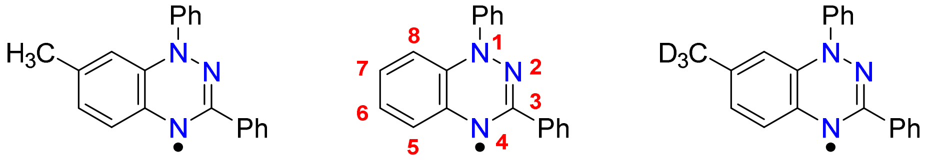

1 **2** **3**

Figure 1. Structures of the studied Blatter radicals; 7-H_3C (**1**), parent system (**2**) and 7-D_3C (**3**).

Herein, we take a deeper look at the mechanistic origins of methyl-driven OE DNP by quantifying contributions from methyl rotation, libration, and quantum tunneling, all of which have the potential to mediate cross-relaxation. We summarize the methyl rovibrational wavefunction and use it to predict the temperature dependence of the cross-relaxation rates and DNP enhancements from the various mechanisms. We then perform ultra-low temperature (ULT) MAS-DNP and EPR experiments to study the temperature dependence of methyl-driven OE DNP and how it relates to the theoretical predictions.

II. Theory

A. Methyl Dynamics

If we ignore bending and stretching modes, which typically occur at frequencies of 90 and 45 THz, respectively, there are two basic motions that a methyl group can undertake: rotation and libration (Figure 2a,b). Furthermore, it is well-known that methyl groups undergo a third type of motion at low temperatures, namely, the quantum tunneling between rotational ground states (Figure 2c).[35-40] The rates at which these motions occur is primarily determined by the sample temperature and the free energy barrier for the rotation ($\Delta G^{\ddagger}_{\text{rot}}$).

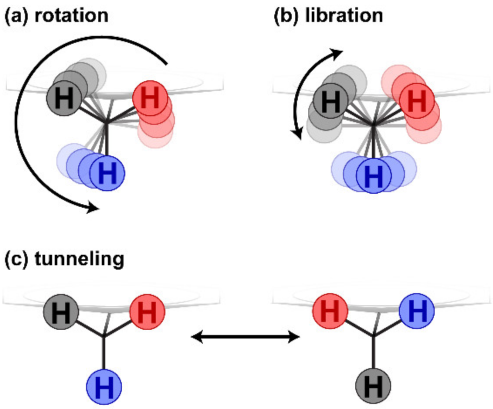

Figure 2. The three dynamic modes that affect methyl groups and can lead to cross-relaxation: (a) rotation, (b) libration, and (c) quantum tunneling.

Due to the three-fold symmetry of the moiety, we can approximate the potential energy surface using the following 2π/3-periodic function (Figure 3a).[35,41]

$$V(\varphi) = \Delta G^{\ddagger}_{\text{rot}}[1 - \cos 3\varphi]/2\ . \tag{1}$$

Classical rotation can be treated as normal kinetics, with a rate (f_{rot}) that depends on the free energy barrier as follows.

$$f_{\text{rot}} = \frac{k_{\text{B}}T}{h} \exp\left(-\frac{\Delta G^{\ddagger}_{\text{rot}}}{RT}\right) \tag{2}$$

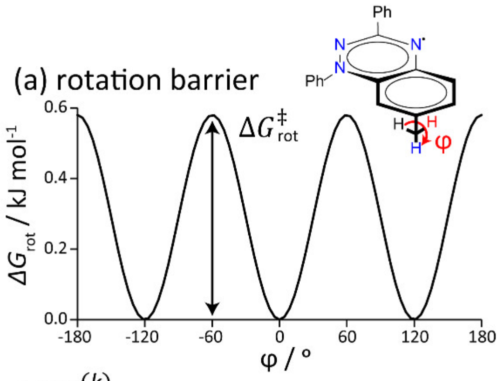
(a) rotation barrier

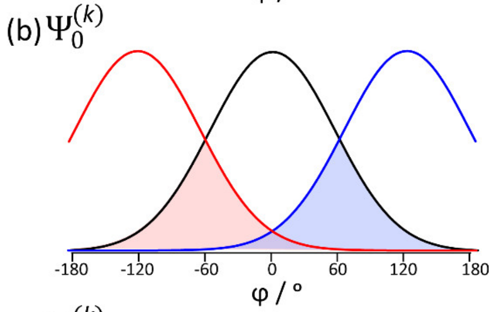
(b) $\Psi_0^{(k)}$

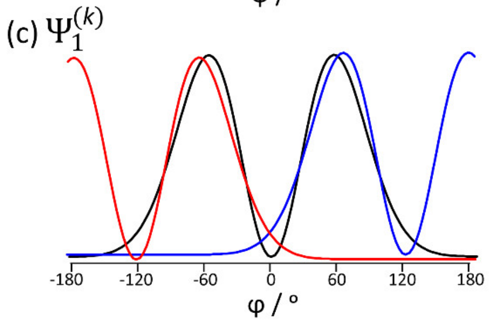
(c) $\Psi_1^{(k)}$

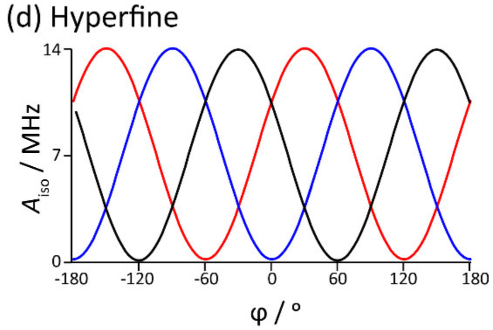
(d) Hyperfine

Figure 3. (a) Rotational potential free energy surface. (b) Representation of the rovibrational ground state, plotted as a function of the methyl rotation phase away from the lowest-energy orientation (φ). Shaded areas depict the overlap between adjacent states (k) that is responsible for methyl tunneling. (c) First excited rovibrational state. (d) Dependence of the isotropic hyperfine coupling on φ for each of the three values of k.

In equation 2, k_B corresponds to the Boltzmann constant, T is temperature, h is Plank's constant, and R is the gas constant. To calculate the librational and tunneling frequencies, it is necessary to consider the quantum mechanical nature of these motions. Using a Taylor expansion of the potential energy surface from equation 1 around the minimum, truncated at second order, Benetis and co-workers obtained librational eigenstates of the form:[41]

$$\Psi_{\nu}^{(k)}(\varphi) = N_{\nu} H_{\nu}(x_k) \exp(-x_k^2/2) \tag{3}$$

where H_v are Hermite polynomials, v are the rovibrational quantum numbers, and k refers to the one of three wells in the potential energy surface situated at

$$\vartheta_k = 2k\pi/3. \tag{4}$$

x_k is given by the following expression:

$$x_k = \sqrt{\beta(\varphi - \vartheta_k)}. \tag{5}$$

The normalization factors are given by:

$$N_{\nu} = \left(\frac{\sqrt{\beta}}{2^{\nu}\sqrt{\pi}\nu!}\right)^{1/2} \tag{6}$$

where β is an angle scaling factor given by the following expression.

$$\beta = \frac{3}{2}\sqrt{\frac{\Delta G_{\mathrm{rot}}^{\ddagger}}{B}} \tag{7}$$

B is the rotational constant, equal to 0.655 meV for a H_3C moiety and 0.328 meV for a D_3C moiety. The two lowest-energy librational wavefunctions are depicted in Figure 3b,c. The librational frequency ($f_{\nu,\mathrm{lib}}$) is easily determined as the energy of the occupied librational state.

$$f_{\nu,\mathrm{lib}} = 2\beta B(\nu + 1/2)/h \tag{8}$$

The tunneling frequency ($f_{0,\mathrm{tunnel}}$) is proportional to the overlap between ground librational states (shaded areas in Figure 3b)

$$\left\langle \Psi_0^{(k)} \middle| \Psi_0^{(k\pm 1)} \right\rangle = \exp\left(-\frac{\pi^2}{6}\sqrt{\frac{\Delta G_{\mathrm{rot}}^{\ddagger}}{B}}\right) \tag{9}$$

and can be approximated by the following expression introduced by Benetis and co-workers.[41]

$$f_{0,\mathrm{tunnel}} = \frac{3\Delta G_{\mathrm{rot}}^{\ddagger}}{2} \exp\left(-\frac{\pi^2}{6}\sqrt{\frac{\Delta G_{\mathrm{rot}}^{\ddagger}}{B}}\right)\left[1 - \frac{3\pi^2}{2} - \frac{9}{2}\sqrt{\frac{B}{\Delta G_{\mathrm{rot}}^{\ddagger}}} + \exp\left(-\frac{3}{2}\sqrt{\frac{B}{\Delta G_{\mathrm{rot}}^{\ddagger}}}\right)\right] \tag{10}$$

B. Methyl-Driven Cross-Relaxation

We will assume that all motions are stochastic and can be characterized by a normalized autocorrelation (G) function of the form:

$$G(t) = \exp(-|t|/\tau_{\mathrm{c}}) \tag{11}$$

which leads to a Lorentzian spectral density function (J).

$$J(\omega) = \frac{\tau_c}{1+\omega^2\tau_c^2} \tag{12}$$

In the above equations, ω corresponds to a particular angular frequency, and J is its relative probability given the correlation time τ_c. The correlation time is the inverse of the dynamics responsible for the relaxation.

$$\tau_{c,\mathrm{mech}} = f_{\mathrm{mech}}^{-1} \tag{13}$$

If the motions induce a modulation of the hyperfine coupling with an amplitude of $\langle A^2 \rangle$, then relaxation-induced transition probabilities (W_m) can be calculated as:[23,42]

$$W_{1e} = \frac{3}{20}\langle A^2 \rangle J(\omega_e) \tag{14}$$

$$W_{1n} = \frac{3}{20}\langle A^2 \rangle J(\omega_n) \tag{15}$$

$$W_0 = \frac{1}{10}\langle A^2 \rangle J(\omega_e - \omega_n) \approx \frac{1}{10}\langle A^2 \rangle J(\omega_e) \tag{16}$$

$$W_2 = \frac{3}{5}\langle A^2 \rangle J(\omega_e + \omega_n) \approx \frac{3}{5}\langle A^2 \rangle J(\omega_e) \tag{17}$$

where ω_e and ω_n are the electron and nuclear Larmor frequencies. The cross- and self-relaxation rates ($R_{e,n}$, $R_{e,e}$, and $R_{n,n}$) are obtained by applying equations 18-20.

$$R_{e,n} = W_2 - W_0 = \frac{1}{2}\langle A^2 \rangle J(\omega_e) \tag{18}$$

$$R_{e,e} = W_0 + 2W_{1e} + W_2 = \langle A^2 \rangle J(\omega_e) \tag{19}$$

$$R_{n,n} = W_0 + 2W_{1n} + W_2 = \frac{7}{10}\langle A^2 \rangle J(\omega_e) + \frac{3}{10}\langle A^2 \rangle J(\omega_n) \tag{20}$$

To estimate the amplitude of the hyperfine modulation in the classical and tunneling-based rotation mechanisms, we assume a 3-site jump mechanism.

$$\langle A^2 \rangle_{\mathrm{rot/tunnel}} = \left(A_{\max} - \frac{\sum_k (A_k)}{3}\right)^2 \tag{21}$$

The rates of the motions (equations 2, 8, and 10) can be used to calculate the correlation times and cross-relaxation rates.

$$R_{e,n,\mathrm{rot}} = \frac{1}{2}\langle A^2 \rangle_{\mathrm{rot}} J_{\mathrm{rot}}(\omega_e) \tag{22}$$

It is also important to also account for the ground state populations (p_0) in the case of tunneling (more on this in section II.C).

$$p_0 = \frac{\exp\left(-\frac{f_{0,\mathrm{lib}}}{k_\mathrm{B}T}\right)}{\sum_\nu \exp\left(-\frac{f_{\nu,\mathrm{lib}}}{k_\mathrm{B}T}\right)} \tag{23}$$

The amplitude of the hyperfine coupling modulation caused by librations is dependent upon *v* and given by the following expression:

$$\langle A^2\rangle_{\nu,\mathrm{lib}} = \left[\frac{\int_{-\pi}^{-\pi}\int_{-\pi}^{\pi} 2\left|\left|\Psi_\nu^{(k)}\right|^2(\varphi_1)\left|\Psi_\nu^{(k)}\right|^2(\varphi_2)\left(A_k(\varphi_1)-(\varphi_2)\right)\right| d\varphi_1 d\varphi_2}{\int_{-\pi}^{-\pi}\int_{-\pi}^{\pi} 2\left|\left|\Psi_\nu^{(k)}\right|^2(\varphi_1)\left|\Psi_\nu^{(k)}\right|^2(\varphi_2)\right| d\varphi_1 d\varphi_2}\right]^2 \tag{24}$$

where, from prior DFT calculations[28] we can approximate *A*(*φ*) as:

$$A_k(\varphi) = A_\mathrm{max}\cos^2(\varphi - \vartheta_k) \tag{25}$$

It may be necessary to consider all rovibrational states and their populations to calculate the cross- and self-relaxation rates from librations.

C. Effect of Combined Motions

Where multiple sets of motions lead to relaxation (rotation, libration, tunneling), the usual approximation is to assume that the individual dynamic modes are uncorrelated such that the total normalized autocorrelation function becomes the product of each individual normalized autocorrelation function.[43]

$$G_\mathrm{total}(t) = \prod\nolimits_\mathrm{i} G_\mathrm{i}(t) \tag{26}$$

This leads to a convolution of the spectral density functions, effectively shortening correlation times.

$$\tau_\mathrm{c,total}^{-1} = \sum\nolimits_\mathrm{i} \tau_\mathrm{c,i}^{-1} \tag{27}$$

These expressions are strictly valid when considering the combination of rotation and tunneling mechanisms at the low-temperature limit because they have the same modulation amplitudes ($\langle A^2\rangle$).

$$\langle A^2\rangle_\mathrm{total\ rot} = \langle A^2\rangle_\mathrm{rot} = \langle A^2\rangle_\mathrm{tunnel} \tag{28}$$

$$\tau_\mathrm{c,total\ rot}^{-1} = \tau_\mathrm{c,rot}^{-1} + \tau_\mathrm{c,tunnel}^{-1} \tag{29}$$

However, in cases where $p_0 < 1$, *i.e.*, at temperatures significantly above absolute zero, it is necessary to consider the ground state population through the application of Lipari-Szabo theory.[44] In this case, the spectral density function for the combined rotation mechanisms becomes:

$$J_\mathrm{total\ rot}(\omega) = \frac{(1-p_0)\tau_\mathrm{c,rot}}{1+\omega^2\tau_\mathrm{c,rot}^2} + \frac{p_0\tau_\mathrm{c,total\ rot}}{1+\omega^2\tau_\mathrm{c,total\ rot}^2}. \tag{30}$$

Unfortunately, simultaneously treating librations and rotations is more complex due to their different hyperfine coupling modulation amplitudes. Here, we chose to apply a modified Lipari-Szabo relaxation model with a $\langle A^2 \rangle$-weighted average of the correlation rates and amplitudes. This solution agrees with equations 26-30 in the limit where the motional amplitudes are equal, which is nearly satisfied in the example studied here. Because the v = 0 state is overwhelmingly responsible for cross-relaxation, we negate the librational excited states.

$$\langle A^2 \rangle_{\text{total}} = \frac{\langle A^2 \rangle_{\text{rot}}^2 + \langle A^2 \rangle_{\text{tunnel}}^2 + \langle A^2 \rangle_{0,\text{lib}}^2}{\langle A^2 \rangle_{\text{rot}} + \langle A^2 \rangle_{\text{tunnel}} + \langle A^2 \rangle_{0,\text{lib}}} \tag{31}$$

$$\tau_{\text{c,total}}^{-1} = \frac{\langle A^2 \rangle_{\text{rot}} \tau_{\text{c,rot}}^{-1} + \langle A^2 \rangle_{\text{tunnel}} \tau_{\text{c,tunnel}}^{-1} + \langle A^2 \rangle_{0,\text{lib}} \tau_{\text{c,0,lib}}^{-1}}{\langle A^2 \rangle_{\text{rot}} + \langle A^2 \rangle_{\text{tunnel}} + \langle A^2 \rangle_{0,\text{lib}}} \tag{32}$$

The spectral density function encompassing all three relaxation mechanisms then becomes:

$$\langle A^2 \rangle J_{\text{total rot}}(\omega) = \langle A^2 \rangle_{\text{rot}} \frac{(1-p_0)\tau_{\text{c,rot}}}{1+\omega^2 \tau_{\text{c,rot}}^2} + \langle A^2 \rangle_{\text{total}} \frac{p_0 \tau_{\text{c,total}}}{1+\omega^2 \tau_{\text{c,total}}^2}. \tag{33}$$

Equation 33 is then used together with equations 18-20 to predict cross- and self-relaxation rates resulting from the combined dynamics of rotation, tunneling, and librations.

At this point, it is important to reiterate the approximations made in the above descriptions. First, we assume that all motions are stochastic. This approximation was shown to be incorrect in the case of BDPA, which has a shifted spectral density function.[23,24] We could expect librations to lead to a similar shift; however, prior variable-field data on the 7-H_3C Blatter radical variant, **1**, suggest our assumption may be valid.[28] Second, the Lipari-Szabo model assumes that all motions are not correlated and can be treated independently, which is also not necessarily true.[45] Lastly, we apply DFT calculations for predicting the values of A_{max}, A_{min}, $\Delta H_{\text{rot}}^{\ddagger}$, and $\Delta S_{\text{rot}}^{\ddagger}$. The calculated enthalpies and entropies have large errors associated to them due to their small magnitudes. Small changes in $\Delta S_{\text{rot}}^{\ddagger}$ in particular can have significant impacts on the predicted temperature-dependence of the relaxation processes. Due to these approximations, theoretical predictions are useful to gauge the expected behaviors of cross-relaxation mechanisms but are not expected to reproduce experimental results quantitatively. As such, we will perform experiments geared towards the distinction of the three main cross-relaxation mechanisms and use the theory exclusively to predict trends.

III. Results and Discussion

A. ^{1}H OE MAS-DNP

We dissolved the radical **1** in a 95:5 mixture of polystyrene (PS)-d8:PS-d5 with a radical concentration of approximately 0.5 % w/w. This matrix was selected due to polystyrene's high glass transition temperature and our inability to flash-freeze samples on the ULT-MAS-DNP NMR spectrometer.[46-50] A similar matrix was also applied successfully to study Overhauser effects at very low temperatures in BDPA.[51]

The sample was packed in a 3.2 mm Si_3N_4 MAS rotor and spun to ~6.5 kHz in a magnetic field of 16.4 T. A narrow sweep of the microwave frequency was first performed to locate the optimal frequency for OE MAS-DNP, following which the temperature was varied from 80 to 18 K. The DNP build-up times (T_{DNP}) and enhancement factors ($\varepsilon_{on/off}$) were measured at each 10 K increment. Example spectra acquired with the microwave beam switched on and off, in addition to plots of the enhancement factor and build-up times, are shown in Figure 4. As can be seen, the enhancement increases monotonically from a value of 2.4 at 81 K to 5.3 at 18 K, while build-up times increase from 3.4 to 14.5 s. The continuous increase in the enhancement factors down to 18 K is counterintuitive, given that one would expect the methyl group to stop rotating at these temperatures.[28]

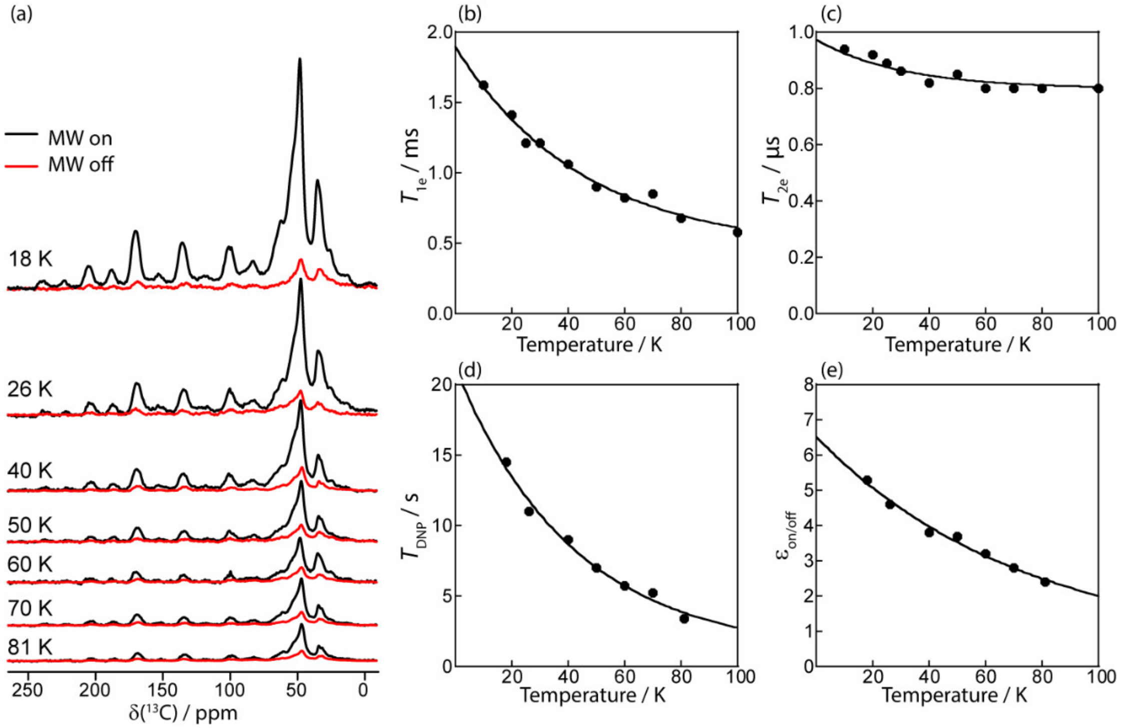

Figure 4. (a) $^{13}C\{^1H\}$ CPMAS NMR spectra acquired for a 95:5 PS-d8:PS-d5 solid solution containing 0.5% w/w radical **1** as a function of temperature, both with and without microwave irradiation. Depending on the temperature, 16 to 512 scans were averaged with the microwave irradiation, and 16 to 2560 scans without irradiation. Electron T_{1e} (b) and T_{2e} (c) measured for the same sample at a 3.4 T magnetic field as a function of temperature. (c) Temperature dependence of the DNP build-up times (c) and enhancement factors (d).

High-field (3.4 T, 94 GHz) EPR measurements were also performed on the sample to measure the temperature dependence of the electron relaxation times (T_{1e} and T_{2e}, Figure 4). The longitudinal relaxation time, T_{1e}, increases exponentially from 0.58 ms at 100 K to 1.62 ms at 10 K. In the range from 80 to 20 K, the T_{1e} lengthened by a factor of 2, while the transverse relaxation time, T_{2e}, was essentially constant. In all, the saturation factor ($s = T_{1e} \cdot T_{2e}$) increased by a factor of only 2.4 from 80 to 20 K while the DNP enhancement factor increased by a factor of 3.1 (from

140% to 430%). As such, we cannot ascribe the observed increase OE DNP efficiency exclusively to a higher electron saturation factor,[13,52] particularly when dynamics are also changing.

B. Predicted OE DNP Performance

To explain the unexpected increase in the DNP enhancements when decreasing the sample temperature to 18 K, we performed a theoretical analysis of the Overhauser DNP processes. DFT calculations were performed on a single 7-H_3C Blatter radical analogue **1** molecule in the gas phase. The structure of the lowest and highest rotational energy conformers was optimized, and normal modes were calculated to predict the molecule's entropy. The $\Delta H^{\ddagger}_{\mathrm{rot}}$ value was predicted to equal 0.58 kJ/mol while no entropy change was predicted, meaning that $\Delta G^{\ddagger}_{\mathrm{rot}}$ should be temperature-independent and equal 0.58 kJ/mol (Figure 3a). The computed isotropic hyperfine coupling A_{iso} is strongly modulated with an amplitude of 14 MHz, as described in our earlier publication. This leads to $\langle A^2 \rangle_{\mathrm{rot}}$ and $\langle A^2 \rangle^2_{0,\mathrm{lib}}$ values of 53 and 62 MHz^2.

This barrier leads to predictions in the tunneling and librational ground state frequencies of 161 and 678 GHz;[41] both of which are close to the typical EPR frequencies of commercial MAS-DNP spectrometers. In the case of a deuterated methyl group in radical **3**, these frequencies are reduced to 17 and 479 GHz, due to the larger rotational constant. These frequencies are temperature-independent, while the rotational frequency needs to be calculated using equation 2 and equals 1 THz at 100 K, 390 GHz at 60 K, and only 13 GHz at 20 K.

Using these values, we can predict the ^{1}H electron cross-relaxation rates (Figure 5a). All three dynamic modes are expected to lead to significant cross-relaxation with rotation, libration, and tunneling individually causing cross-relaxation rates of 21, 21, and 9 Hz at 100 K. As we reduce the temperature all three mechanisms increase in efficiency until 65 K when the maximum rotational cross-relaxation rate is obtained. Librations then surpass rotations as the leading cross-relaxation mechanism at 55 K and remain dominant down to 0 K, with roughly twice the efficiency of tunneling. The total cross-relaxation rate is remarkably constant varying only from 25 to 33 Hz.

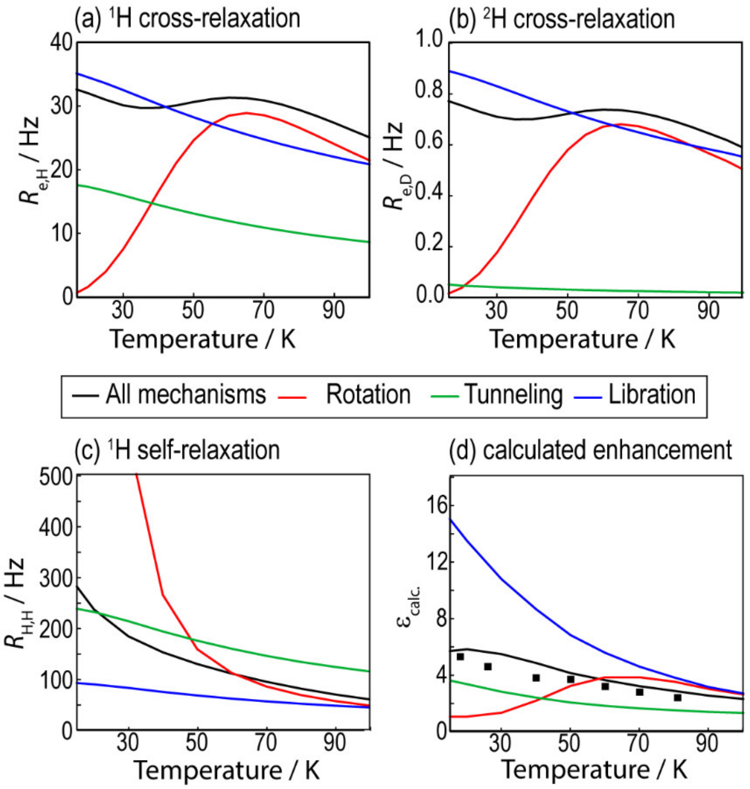

Figure 5. Temperature dependence of the ^{1}H (a) and ^{2}H (b) electron-nuclear cross-relaxation rates, and ^{1}H self-relaxation rates (c) calculated using rotation barriers obtained from DFT for radicals **1** and **3**. (d) Calculated temperature dependence of the ^{1}H OE DNP enhancements for a model consisting of a periodic 0.5 % w/w radical **1** solution in 5% PS-d5, with a single radical in the repeating unit (1 electron, 100 protons). Experimental enhancements are added for comparison purposes.

The story is very much the same in the case of D_3C moieties in radical **3**, except that deuteration largely quenches the tunneling mechanism, reducing it to 1/18th the efficiency of the librational cross-relaxation rate. As such, deuteration is a useful approach to distinguish between librations and tunneling, which otherwise have the same predicted temperature dependence.

Spin dynamics calculations were applied to predict the temperature dependence of ^{1}H Overhauser MAS-DNP. The model consisted of a periodic 4.54 nm box with one 7-H_3C Blatter radical **1**, and 28 polystyrene-d5 monomers distributed at random. This arrangement was chosen to mimic the experiments as closely as possible. Calculations employed our hybrid quantum-classical MAS-DNP simulation model[53-55] that combines a kinetic treatment of spin diffusion[56] with the Landau-Zener description of MAS-DNP.[57,58] Briefly, the density operator ($\hat{\sigma}$) is propagated as:

$$\hat{\sigma}(t) = \prod_{\mathrm{p}=0}^{\mathrm{P}} \left[\hat{\hat{U}}_{\mathrm{LZ}}(t_{\mathrm{p}}) \cdot \exp\left[\left(\hat{\hat{R}}_{1,2}(t_{\mathrm{p}}) + \hat{\hat{R}}_{\mathrm{OE}} + \hat{\hat{K}}\right)\Delta t\right]\right]\hat{\sigma}(0) \qquad (34)$$

where $\hat{\hat{U}}_{\mathrm{LZ}}$ is the Landau-Zener MAS-DNP propagator that describes electron saturation during microwave MAS rotor events, $\hat{\hat{R}}_{1,2}$ is the relaxation superoperator, $\hat{\hat{R}}_{\mathrm{OE}}$ is the OE superoperator, and $\hat{\hat{K}}$ is the exchange rate matrix describing spin diffusion. The exact forms of these matrices are given in earlier publications.[53,55,58] Experimental DNP built-up times (T_{DNP}) and $T_{1\mathrm{e}}$ values were used along with the predicted cross- and self-relaxation rates. The microwave power was set to 100 kHz and the spin diffusion rates were calculated using the following hyperfine-dependent expression described in ref. 53:

$$k_{\mathrm{i,j}} = \frac{A R_{\mathrm{DD,i,j}}^{2}}{\nu_{\mathrm{r}} + B\left(\sum_{\mathrm{electrons}} A_{\mathrm{zz,PAS,i}} A_{\mathrm{zz,PAS,j}}\right)^{C/2}} \tag{35}$$

where $A_{\mathrm{zz,PAS}}$ corresponds to the largest principal component of the hyperfine coupling tensor and includes the isotropic part, ν_{r} is the MAS frequency, and R_{DD} is the ^{1}H-^{1}H dipolar coupling constant. A, B, and C are adjustable parameters used to tune the behavior of the spin diffusion. Due to the higher magnetic field strength of the experiments, and the very large isotropic hyperfine coupling constants felt by all the ^{1}H spins on the radical,[28] it was necessary to reduce A and increase B to obtain reasonable results. Their values were set to 0.0005 and 0.01 s^{C-1}, respectively, and C equaled 1.2.

The simulations (Figure 5d) predict that rotation-based OE DNP enhancements should peak at 60 K and sharply decrease in amplitude at lower temperatures. Tunneling-only OE DNP should become more efficient than rotation-only OE DNP at roughly 40 K while libration-only OE enhancements are comparable to the rotation enhancements until 60 K. In aggregate, the simulations predict that the enhancements should increase in amplitude down to absolute zero, primarily due to the changing population of the $v = 0$ ground librational state and increases in nuclear relaxation times. Interestingly, enhancements are predicted to be larger when considering only librations than when incorporating all sets of dynamics. Figure 5c shows the predicted ^{1}H self-relaxation rates as a function of temperature. As the temperature is reduced, rotation-induced self-relaxation of the methyl ^{1}H spins dramatically increases as they slow to around 700 MHz. As such, while the relaxation times of the solvent ^{1}H spins increase by a factor of 4.3 when decreasing the temperature from 80 to 20 K (Figure 4d), enabling them to hold more hyperpolarization, the DNP enhancements only increase by a factor of 2 in both the experiments and simulations (Figure 5d). Due to their faster self-relaxation, the methyl ^{1}H spins are unable to generate as much hyperpolarization, a quatity that should roughly scale with $R_{\mathrm{e,H}}/R_{\mathrm{H,H}}$.

C. ^{2}H OE MAS-DNP

The experimental results and simulations in Figures 4 and 5, respectively, strongly suggest that methyl rotation is not the dominant mechanism leading to the observed cross-relaxation. Instead, it is likely that either quantum tunneling, or librations, are leading the OE DNP in the 7-H_3C Blatter analogue **1**, particularly at very low temperatures. From this data, however, it is not possible to conclusively differentiate between the two mechanisms which predict the same dependence that is proportional to the nuclear T_1 and the population of the $v = 0$ librational state.

As discussed above, and as shown in Figure 5b, one approach to distinguish between tunneling and libration-based cross-relaxation is deuteration. D_3C groups are far less likely to tunnel than H_3C groups, with the predicted tunneling frequency being roughly an order of magnitude lower at 17 GHz instead of 161 GHz for the H_3C. While we have shown that D_3C groups cannot mediate ^{1}H OE DNP, due to the lack of a ^{1}H hyperfine coupling modulation, we have also shown that the 7-D_3C Blatter radical analogue **3** is capable of mediating ^{2}H OE DNP. As such, we have studied the temperature dependence of methyl-driven ^{2}H OE DNP. If tunneling were the dominant cross-relaxation mechanism in the H_3C radical **1**, we would expect the D_3C radical **3** to show a decrease in OE DNP efficiency with decreasing temperature due to the higher relative importance of methyl rotation.

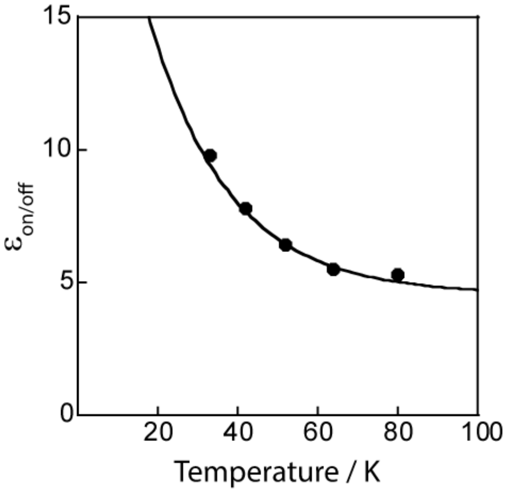

Figure 6. Temperature dependence of the ^{2}H OE DNP enhancement factors acquired for a 5% PS-d_5 0.5% radical **1** solid solution.

The experimental spectra and data are shown in Figure 6. We again see a monotonic increase in DNP efficiency when decreasing the sample temperature from 80 to 33 K. Specifically, ^{2}H OE enhancement factors increased from 5.3 at 80 K to 9.8 at 33 K. As discussed above, this suggests that librations are the dominant cross-relaxation mechanism, which was also the predicted dominant mechanism from the DFT calculations. Importantly, this result suggests that OE DNP may be possible in a broader range of moieties that can undergo librations but not necessarily rotations, such as phenyl groups and CH_2R moieties.

IV. Conclusions

We revisited the mechanism behind methyl-driven Overhauser DNP,[28] considering three different types of dynamics: methyl rotation, libration, and tunneling. While rotation is expected to freeze at very low temperatures, we show that zero-point librations and tunneling appear with frequencies near the EPR frequency and with large enough amplitudes to modulate Overhauser effects. Unlike rotations, these mechanisms are expected to increase in efficiency at lower temperatures due to the population of the librational ground state. Experimentally, at 16.4 T, we observe an increase in DNP efficiency when moving from 80 to 18 K, in agreement with cross-relaxation being dominated by these mechanisms, and not necessarily methyl rotation. An experiment performed on a D_3C-functionalized radical **3**, which should have negligible tunneling, similarly showed increased performance at very low temperatures suggesting that the dominant cross-relaxation mechanism is methyl libration. This result is significant because it suggests that the libration of other, non-rotating, ancillary groups in conjugated radicals could be used to mediate the Overhauser effect and design efficient polarizing agents for ultra-high magnetic fields.

V. Experimental

A. Synthesis

1. General Methods and Materials.

All chemicals were commercially sourced, except those whose synthesis is described. CH_2Cl_2 and THF were freshly distilled from CaH_2 under argon. Reactions were protected from atmospheric moisture by $CaCl_2$ drying tubes. All reaction mixtures and column eluents were monitored by thin-layer chromatography (TLC) using commercial aluminum-backed TLC plates (Merck Kieselgel 60 F_{254} or, where stated). TLC plates were observed under UV light at 254 and 365 nm. The technique of dry flash chromatography[59] was used throughout for all non-TLC-scale chromatographic separations and employed silica gel 60 (<0.063 mm). Melting and decomposition points were determined using either a PolyTherm-A, Wagner & Munz, Koefler–Hostage Microscope apparatus. The solvent used for recrystallization is indicated after each melting point. UV/vis spectra were obtained using a PerkinElmer Lambda-25 UV/vis spectrophotometer. IR spectra were recorded on Shimadzu FTIR-NIR Prestige-21 spectrometer with a Pike Miracle Ge ATR accessory; strong, medium, and weak peaks are represented by “s”, “m”, and “w”, respectively. MALDI-TOF mass spectra were recorded on a Bruker Autoflex III Smartbeam instrument. Elemental analysis was performed on a PerkinElmer 2400 series elemental analyzer at London Metropolitan University. *N*-Phenylbenzohydrazonyl chloride,[60] 7-methyl-1,3-diphenyl-1,4-dihydrobenzo[*e*][1,2,4]-triazin-4-yl (**1**)[61] and 1,3-diphenyl-1,4-dihydrobenzo[*e*][1,2,4]triazin-4-yl (**2**),[29] were prepared according to literature.

2. 7-(Methyl-d_3)-1,3-diphenyl-1,4-dihydrobenzo[*e*][1,2,4]triazin-4-yl (3).[28]

To a stirred solution of *N*-phenylbenzohydrazonyl chloride (537 mg, 2.33 mmol) in anhydrous THF (2.5 mL) at *ca*. 20 °C, were added in single portions triethylamine (324 μL, 2.33 mmol) and then *p*-toluidine-d_3 (249 mg, 2.26 mmol). The mixture was stirred at *ca*. 20 °C for 20 h until the starting materials were fully consumed (TLC, R_f 0.58, *n*-Hex/*t*-BuOMe, 90:10). The solvent was removed *in vacuo* and to the resulting crude was added 2% acetic acid (5 mL). The stirred mixture was heated to *ca.* 70 °C for 1 h and then left to cool, followed by an extraction with CH_2Cl_2 (2 × 15 mL). The organic layer was dried ($MgSO_4$), filtered and the volatiles were removed *in vacuo*. The remaining oily residue was triturated (*c*-hexane, 5 mL) to give crude *N*-(4-methyl-d_3-phenyl)-*N′*-phenylbenzene-carbohydrazonamide (510 mg, 73%) as an off-white powder; mp (hot-stage) 51-53 °C; R_f 0.58 (*n*-Hex/*t*-BuOMe, 90:10); λ_{max} (CH_2Cl_2)/nm 291 (log ε 3.89), 339 (4.16); ν_{max}/cm^{-1} 3333w, 2924w, 2849w, 1599s, 1555w, 1516s, 1506s, 1446w, 1429w, 1392w, 1306w, 1296w, 1244m, 1282w, 1165m, 1153w, 1078w, 1062w, 1024w, 887w, 869w, 783w, 771m, 750s.

Without further purification, the crude material was converted into the radical. As such, to a stirred solution of *N*-(4-methyl-*d*$_3$-phenyl)-*N′*-phenylbenzenecarbohydrazonamide (151 mg, 0.50 mmol) in anhydrous CH_2Cl_2 (1 mL) at *ca.* 20 °C was added 1,8-diazabicyclo[5.4.0]undec-7-ene (DBU) (7.50 μL, 0.05 mmol) and 5% Pd/C (17.0 mg, 1.60 mol %). The mixture was stirred at *ca.* 20 °C for 18 h until the starting material was fully consumed [TLC, R_f 0.65, (*n*-Hex/*t*-BuOMe, 80:20)]. The solvent was removed *in vacuo,* and the residue was chromatographed (*n*-Hex/*t*-BuOMe 80:20) to give the crude product (80 mg), which was then triturated (*n*-pentane, 4 mL) to give the title compound **3** (70 mg, 46%) as black prisms; mp (hot-stage) 174-176 °C; R_f 0.65 (*n*-Hex/*t*-BuOMe, 80:20); Anal. Calcd. for $C_{20}H_{13}D_3N_3$: C, 79.70; H, 6.35; N, 13.94. Found C, 79.78; H, 6.18; N, 14.01; λ_{max} (CH_2Cl_2)/nm 274 (log ε 4.33), 322 (3.69), 372 (3.64), 430 (3.39), 497 (2.89); ν_{max}/cm^{-1} 3065w & 3027w (aryl CH), 1591w, 1504m, 1491m, 1458w, 1452w, 1422w, 1392s, 1326m, 1277w, 1255w, 1170w, 1158w, 1127w, 1085w, 1067w, 1023w, 1002w, 987w, 918w, 896m, 847w, 779s, 757s, 736w, 704s; *m*/*z* (MALDI) 302 (MH$^+$ 63%), 301 (M$^+$ 100).

B. MAS-DNP

A 0.5% w/w solid solution of radical **1** in 95:5 PS-d8:PS-d5 was prepared by dissolving 1.0 mg of the radical together with 190 mg of PS-d8 and 10 mg of PS-d5 in minimum dichloromethane. Deuterated polymers were obtained from Polymer Source (Montreal, Canada) and used as is. The solution was then cast in a Petrie drish and left to dry. The resulting polymer film was collected and stored in an Ar glovebox to prevent the oxidation of the radical.

The solid solution of radical **1** was packed into a 3.2 mm Si_3N_4 rotor under an argon environment. About 20 mg of the material was center-packed using Kel-f spacers, where one of the spacers was hollowed to house KBr powder used to measure the temperature in the rotor using the ^{79}Br longitudinal relaxation time.[62] The Vespel rotor caps (both turbine cap and bottom cap) are specially designed to tighten at low temperatures while also being easy to remove at ambient temperatures, enabling their repeated use.[63-65]

All ULT-DNP MAS NMR data were recorded with a JEOL RESONANCE, ECA-II spectrometer operating at B_0 = 16.4 T, equipped with a home-built continuous-wave frequency-tunable 460 GHz gyrotron as a sub-millimeter (sub-mm) wave source and a closed-cycle cryogenic helium circulation (CHC)-MAS system together with the dedicated DNP-NMR probe.[47,66] The gyrotron uses a 10 T cryogen-free superconducting magnet (JMTD-10T100, JASTEC), oscillating at the second harmonics mode. In search of the maximum enhancement for the Blatter radical, the frequency of the sub-mm wave was swept between 459.7 and 460.2 GHz. The maximum enhancement was found at 459.92 GHz, where the temperature dependence was recorded. The sample temperature was changed using the heaters installed on the main transfer tubes just before the probe inlets. The MAS rate was fixed (typically to 6.5-6.8 kHz) while measuring the temperature dependence of the enhancement factor.

The ^{1}H, ^{13}C and ^{2}H Larmor frequencies were 698.66, 175.67, and 107.24 MHz, respectively. The ^{1}H radiofrequency (RF) amplitudes were set to 70, 33 and 70 kHz, respectively, for the excitation, CP contact, and ^{1}H decoupling pulses. The ^{13}C RF amplitude was 25 kHz for the CP contact. For ^{2}H, the excitation pulse length was 40 µs with a power of 155 W. The ^{2}H tuning was achieved using a frequency splitter (REDOR box) on the X channel. However, the circuit efficiency was insufficient, and no magnetization nutation or saturation was observed. Thus, the RF field strength and the relaxation time could not be measured for ^{2}H.

C. EPR Spectroscopy

The W-band (94 GHz, 3.4 T) T_{1e} and T_{2e} values were measured using the HiPER (High Power quasi-optical EPR) spectrometer located at the National High Magnetic Field Laboratory (NHMFL) in Tallahassee, Florida. This high microwave power spectrometer is an upgraded version[67] of the original instrument developed at the University of St. Andrews[68] designed to measure short electron relaxation times in large sample volume such as the ones used in DNP experiments. The helium flow cryostat permits variable temperature measurements from 5 K to room temperature. T_{2e} values were measured using a Hahn echo sequence with 50 and 100 ns excitation and refocusing pulse widths (2W of power). T_{1e} measurements utilized the same sequence with the addition of a long, 10 µs, saturation pulse.

D. Density Functional Theory

A molecular model for the 7-H_3C Blatter-type radical was constructed using Amsterdam Modeling Suite graphical user interface (AMS-GUI) ver. 2021.106. All DFT calculations were carried out using the Amsterdam Density Functional (ADF) engine in AMS ver. 2022.102 at the unrestricted PBE0/TZP level of theory[69-71] with scalar relativistic effects included using the zeroth-order regular approximation (ZORA).[72-74] Statistical thermal analyses were obtained by carrying out calculations of the normal modes of vibration. The highest energy structure was obtained by performing a transition state search[75,76] starting with the coordinates of the highest energy structure obtained from a potential energy surface scan over the H-C_{Me}-C_7-C_8 dihedral angle (φ).[28]

E. Spin Dynamics Simulations

Spin dynamics calculations of DNP processes were performed using an in-house C program described in detail elsewhere.[48-50] The lowest-energy structure for the 7-H_3C Blatter radical analogue was used with the electron spin assumed to be localized in the center of the C5-C8 aromatic ring. DFT calculated isotropic and anisotropic hyperfine coupling constants were used for all ^{1}H nuclei within the radical molecule while intermolecular interactions were assumed to be purely dipolar and defined by the distance to this point spin. The radical molecule was randomly inserted into a periodic box with dimensions of 45.47 Å after which 28 RCH_2-CHR_2 fragments were randomly added to the box to emulate the partially deuterated polystyrene matrix. The coordinates of the model are given in the supplementary information.

Nuclear spin diffusion was defined using equations 34 and 35 and bulk relaxation times were simply set to the T_{DNP} values (see supplementary information). Nuclear relaxation times were further damped in accordance to their proximity to the radical using equation 36, with the relaxation time at 1 Å from the radical set to 0.1 s.

$$\frac{1}{T_1} = \frac{1}{T_{\mathrm{DNP}}} + \frac{1\text{Å}^6}{T_{1,1\text{Å}}r^6} \qquad (36)$$

The MAS frequency was set to 10 kHz, the ^{1}H Larmor frequency to 700 MHz, and the microwave frequency to 460.965 GHz. The microwave power equaled 100 kHz. The electron *g* tensor principal components were set to 2.0043, 2.0035, and 2.0015 to agree with previously reported values for Blatter radicals.[77] Cross and self-relaxation times were set to the values calculated in this work and plotted in Figure 4. Powder averaging was achieved using a 66-orientation REPULSION grid.[78] Reported computed DNP enhancements are the average values for all PS-d5 ^{1}H spins and explicitly exclude ^{1}H spins from the radical molecule.

Supplementary Material

See supplementary material for the ^{2}H NMR spectra, Tables of the experimental DNP enhancements, build-up times, electron relaxation times, and the predicted cross- and self-relaxation rates. Coordinates are also provided for the model used in the spin dynamics simulations in addition to those from the lowest-energy and transition state structures calculated using DFT.

Acknowledgements

Prof. Aaron Rossini is thanked for numerous insightful discussions. This work was supported by Laboratory-Directed Research and Development at Ames Laboratory. The spin dynamics simulations were supported by the U.S. Department of Energy, Office of Science, Basic Energy Sciences, Materials Science and Engineering Division. The Ames National Laboratory is operated for the U.S. DOE by Iowa State University under Contract No. DE-AC02-07CH11358. MAS-DNP experiments (YM) were supported by JST SENTAN (H271030 and JPMJSN15A1), A-STEP(JPMJTR204D), and the Ministry of Education, Culture, Sports, Science and Technology (MEXT), Japan (480790). EPR experiments (TB and JVT) were supported by the National Science Foundation (grants numbers DMR-1644779 and DMR-2128556) as well as the State of Florida. C.P.C. (synthesis) thanks the University of Michigan-Dearborn for an UM-Dearborn Scholars award. P.A.K. and D.F.F. (synthesis) thank the University of Cyprus for the internal grant THOR-PHOTO, the A. G. Leventis Foundation for helping to establish the NMR facility at the University of Cyprus, the Cyprus Research Promotion Foundation and the following organizations and companies in Cyprus for generous donations of chemicals and glassware: the State General Laboratory, the Agricultural Research Institute, the Ministry of Agriculture, MedoChemie Ltd., Medisell Ltd., Biotronics Ltd.

Data Availability

Experimental enhancements and relaxation time constants are tabulated in the supplementary material together with cross-relaxation rates used for the simulations. The atomic coordinates used for the spin dynamics and DFT calculations are also given as supplementary information. The most recent version of the source code used for the DNP simulations can be obtained from the authors, as well as the raw NMR data.

References

---

[1] T. Maly, G. T. Debelouchina, V. S. Bajaj, K.-N. Hu, C.-G. Joo, M. L. Mak-Jurkauskas, J. R. Sirigiri, P. C. A. van der Wel, J. Herzfeld, R. J. Temkin, and R. G. Griffin, J. Chem. Phys. **128**, 052211 (2008).

[2] Y. Su, L. Andreas, and R. G. Griffin, Annu. Rev. Biochem. **84**, 465 (2015).

[3] Ü. Akbey and H. Oschkinat, J. Magn. Reson. **269**, 213 (2016).

[4] T. Biedenbänder, V. Aladin, S. Saeidpour, and B. Corzilius, Chem. Rev. **122**, 9738 (2022).

[5] W. Y. Chow, G. De Paëpe, and S. Hediger, Chem. Rev. **122**, 9795 (2022).

[6] A. J. Rossini, A. Zagdoun, M. Lelli, A. Lesage, C. Copéret, and L. Emsley, Acc. Chem. Res. **46**, 1942 (2013).

[7] T. Kobayashi, F. A. Perras, I. I. Slowing, A. D. Sadow, and M. Pruski, ACS Catal. **5**, 7055 (2015).

[8] W.-C. Liao, B. Ghaffari, C. P. Gordon, J. Xu, and C. Copéret, Curr. Opin. Colloid Interface Sci. **33**, 63 (2018).

[9] A. G. M. Rankin, J. Trébosc, F. Pourpoint, J.-P. Amoureux, and O. Lafon Solid State Nucl. Magn. Reson. **101**, 116 (2019).

[10] C. D. Jeffries, Phys. Rev. **106**, 164 (1957).

[11] M. Abraham, R. W. Kedzie, and C. D. Jeffries, Phys. Rev. **106**, 165 (1957).

[12] C. F. Hwang and D. A. Hill, Phys. Rev. Lett. **18**, 110 (1967).

[13] A. W. Overhauser, Phys. Rev. **92**, 411 (1953).

[14] T. R. Carver and C. P. Slichter, Phys. Rev. **92**, 212 (1953).

[15] K.-N. Hu, H.-h. Yu, T. M. Swager, and R. G. Griffin J. Am. Chem. Soc. **126**, 10844 (2004).

[16] C. Song, K.-N. Hu, C.-G. Joo, T. M. Swager, and R. G. Griffin, J. Am. Chem. Soc. **128**, 11385 (2006).

[17] Y. Matsuki, T. Maly, O. Ouari, H. Karoui, F. Le Moigne, E. Rizzato, S. Lyubenova, J. Herzfeld, T. Prisner, P. Tordo, R. G. Griffin, Angew. Chem. Int. Ed. **48**, 4996 (2009).

[18] A. Zagdoun, G. Casano, O. Ouari, M. Schwarzwälder, A. J. Rossini, F. Aussenac, M. Yulikov, G. Jeschke, C. Copéret, A. Lesage, P. Tordo, and L. Emsley, J. Am. Chem. Soc. **135**, 12790 (2013).

[19] C. Sauvée, M. Rosay, G. Casano, F. Aussenac, R. T. Weber, O. Ouari, and P. Tordo, Angew. Chem. Int. Ed. **52**, 10858 (2013).

[20] G. Mathies, M. A. Caporini, V. K. Michaelis, Y. Liu, K.-N. Hu, D. Mance, J. L. Zweier, M. Rosay, M. Baldus, and R. G. Griffin, Angew. Chem. Int. Ed. **54**, 11770 (2015).

[21] F. Mentink-Vigier, I. Marin-Montesinos, A. P. Jagtap, T. Halbritter, J. van Tol, S. Hediger, D. Lee, S. T. Sigurdsson, and G. De Paëpe, J. Am. Chem. Soc. **140**, 11013 (2018).

[22] T. V. Can, M. A. Caporini, F. Mentink-Vigier, B. Corzilius, J. J. Walish, M. Rosay, W. E. Maas, M. Baldus, S. Vega, T. M. Swager, and R. G. Griffin, J. Chem. Phys. **141**, 064202 (2014).

[23] S. Pylaeva, K. L. Ivanov, M. Baldus, D. Sebastiani, and H. Elgabarty, J. Phys. Chem. Lett. **8**, 2137 (2017).

[24] S. Pylaeva, P. Marx, G. Singh, T. D. Kühne, M. Roemelt, and H. Elgabarty, J. Phys. Chem. A **125**, 867 (2021).

[25] A. Gurinov, B. Sieland, A. Kuzhelev, H. Elgabarty, T. D. Kühne, T. Prisner, J. Paradies, M. Baldus, K. L. Ivanov, and S. Pylaeva, Angew. Chem. Int. Ed. **60**, 15371 (2021).

[26] L. Delage-Laurin, R. S. Palani, N. Golota, M. Mardini, Y. Ouyang, K. O. Tan, T. M. Swager, and R. G. Griffin, J. Am. Chem. Soc. **143**, 20281 (2021).

---

[27] R. S. Palani, M. Mardini, L. Delage-Laurin, D. Banks, Y. Ouyang, E. Bryerton, J. G. Kempf, T. M. Swager, and R. G. Griffin, J. Phys. Chem. Lett. **14**, 95 (2023).

[28] F. A. Perras, D. F. Flesariu, S. A. Southern, C. Nicolaides, J. D. Bazak, N. M. Washton, T. Trypiniotis, C. P. Constantinides, and P. A. Koutentis, J. Phys. Chem. Lett. **13**, 4000 (2022).

[29] H. M. Blatter and H. Lukaszewski, Tetrahedron Lett. **9**, 2701 (1968).

[30] C. P. Constantinides, P. A. Koutentis, and G. Loizou, Org. Biomol. Chem. **9**, 3122 (2011).

[31] A. A. Berezin, G. Zissimou, C. P. Constantinides, Y. Beldjoudi, J. M. Rawson, and P. A. Koutentis, J. Org. Chem. **79**, 314 (2014).

[32] C. P. Constantinides, E. Obijalska, and P. Kaszyński, Org. Lett. **18**, 916 (2016).

[33] A. C. Savva, S. I. Mirallai, G. A. Zissimou, A. A. Berezin, M. Demetriades, A. Kourtellaris, C. P. Constantinides, C. Nicolaides, T. Trypiniotis, and P. A. Koutentis, J. Org. Chem. **82**, 7564 (2017).

[34] T. Maly, D. Cui, R. G. Griffin, and A.-F. Miller, J. Phys. Chem B. **116**, 7055 (2012).

[35] E. O. Stejskal and H. S. Gutowski, J. Chem. Phys. **28**, 388 (1958).

[36] C. D. Knutson and D. M. Spitzer Jr, J. Chem. Phys. **45**, 407 (1966).

[37] S. Clough, Sci. Prog. **75**, 121 (1991).

[38] M. Prager, H. Grimm, and I. Natkaniec, Phys. Chem. Chem. Phys. **7**, 2587 (2005).

[39] M. Šimėnas, D. Klose, M. Ptak, K. Aidas, M. Mączka, J. Banys, A. Pöppl, and G. Jeschke, Sci. Adv. **6**, eaba1517 (2020).

[40] G. Usevičius, A. Eggeling, I. Pocius, V. Kalendra, D. Klose, M. Mączka, A. Pöppl, J. Banys, G. Jeschke, and M. Šimėnas, Molecules **28**, 979 (2023).

[41] N. P. Benetis, I. A. Zelenetckii, and Y. A. Dmitriev, Low Temp. Phys. **45**, 427 (2019).

[42] M. H. Levitt, Spin Dynamics, John Wiley & Sons, Ltd.: West Sussex (2008).

[43] D. Wallach, J. Chem. Phys. **47**, 5258 (1967).

[44] G. Lipari and A. Szabo, J. Am. Chem. Soc. **104**, 4546 (1982).

[45] M. A. Neumann, M. Plazanet, M. R. Johnson, and H. P. Trommsdorff, J. Chem. Phys. **120**, 885 (2004).

[46] Y. Matsuki, K. Ueda, T. Idehara, R. Ikeda, I. Ogawa, S. Nakamura, M. Toda, T. Anai, and T. Fujiwara, J. Magn. Reson. **225**, 1 (2012).

[47] Y. Matsuki, S. Nakamura, S. Fukui, H. Suematsu, and T. Fujuwaram J. Magn. Reson. **259**, 76 (2015).

[48] Y. Matsuki, T. Idehara, J. Fukazawa, and T. Fujiwara, J. Magn. Reson. **264**, 107 (2016).

[49] Y. Matsuki, T. Kobayashi, J. Fukazawa, F. A. Perras, M. Prusaki, and T. Fujiwara, Phys. Chem. Chem. Phys. **23**, 4919 (2021).

[50] Y. Matsuki, S. Nakamura, F. Hobo, Y. Endo, H. Takahashi, H. Suematsu, and T. Fujiwara, J. Magn. Reson. **335**, 107139 (2022).

[51] X. Ji, T. V. Can, F. Mentink-Vigier, A. Bornet, J. Milani, B. Vuichoud, M. A. Caporini, R. G. Griffin, S. Jannin, M. Goldman, and G. Bodenhausen, J. Magn. Reson. **286**, 138 (2018).

[52] D. J. Cheney and C. J. Wedge, J. Chem. Phys. **152**, 034202 (2020).

[53] F. A. Perras and M. Pruski, J. Chem. Phys. **149**, 154202 (2018).

[54] F. A. Perras, M. Raju, S. L. Carnahan, D. Akbarian, A. C. T. van Duin, A. J. Rossini, and M. Pruski, J. Phys. Chem. Lett. **11**, 5655 (2020).

[55] F. A. Perras, S. L. Carnahan, W.-S. Lo, C. J. Ward, J. Yu, W. Huang, and A. J. Rossini, J. Chem. Phys. **156**, 124112 (2022).

[56] B. Elena and L. Emsley, J. Am. Chem. Soc. **127**, 9140 (2005).

[57] K. R. Thurber and R. Tycko J. Chem. Phys. **137**, 084508 (2012).

---

[58] F. Mentink-Vigier, S. Vega, and G. De Paëpe, Phys. Chem. Chem. Phys. **19**, 3506 (2017).

[59] L. M. Harwood, *Aldrichimica Acta* **18**, 25 (1985).

[60] C. Ghilieri-Bertez, C. Coquelet, A. Alazet and C. Bonne, Eur. J. Med. Chem. **22**, 147 (1987).

[61] P. A. Koutentis and D. Lo Re, Synthesis 2075 (2010).

[62] K. R. Thurber and R. Tycko, J. Magn. Reson. **196**, 84 (2008).

[63] T. Fujiwara, Y. Matsuki, Y. Endo, T. Nemoto, S. Nakamura, Patent JP-6750819-B2 (Aug. 17, 2020).

[64] T. Fujiwara, Y. Matsuki, Y. Endo, T. Nemoto, S. Nakamura, Patent US-10914799-B2 (Feb. 09, 2021).

[65] T. Fujiwara, Y. Matsuki, Y. Endo, T. Nemoto, S. Nakamura, Patent EP-3561532-A1 (Nov. 02, 2022).

[66] Y. Matsuki and T. Fujiwara, EMagRes. **7**, 9 (2018).

[67] M. V. H. Subramanya, J. Marbey, K. Kundu, J. E. McKay, and S. Hill, Appl. Magn. Reson. **54**, 165 (2022).

[68] P. A. S. Cruickshank, D. R. Bolton, D. A. Robertson, R. I. Hunter, R. J. Wylde, and G. M. Smith, Rev. Sci. Instrum. **80**, 103102 (2009).

[69] J. P. Perdew, K. Burke, and M. Ernzerhoff, Phys. Rev. Lett. **77**, 3865 (1996).

[70] J. P. Perdew, M. Ernzerhoff, and K. Burki J. Chem. Phys. **105**, 9982 (1996).

[71] C. Adamo and V. Barone, J. Chem. Phys. **110**, 6158 (1999).

[72] C. Chang, M. Pelissier, and P. Durand, Phys. Script. **34**, 394 (1986).

[73] E. Van Lenthe, E. J. Baerends, and J. G. Snijders, Chem. Phys. **99**, 4597 (1993).

[74] E. Van Lenthe, E. J. Baerends, and J. G. Snijders, J. Chem. Phys. **101**, 9873 (1994).

[75] L. Versluis and T. Ziegler, J. Chem. Phys. **88**, 322 (1988).

[76] L. Fan and T. Ziegler, J. Am. Chem. Soc. **114**, 10890 (1992).

[77] A. S. Poryvaev, E. Gjuzi, D. M. Polyukhov, F. Hoffmann, M. Fröba, M. V. Fedin, Angew. Chem. Int. Ed. **60**, 8683 (2021).

[78] M. Bak and N. C. Nielsem, J. Magn. Reson. **125**, 132 (1997).